Direct external imaging of nascent cancer, tumor progression, angiogenesis, and metastasis on internal organs in the fluorescent orthotopic model

Meng Yang*, Eugene Baranov*, Jin-Wei Wang*, Ping Jiang*, Xiaoen Wang*, Fang-Xian Sun*, Michael Bouvet†, A. R. Moossa†, Sheldon Penman‡, and Robert M. Hoffman*†§

*AntiCancer, Inc., 7917 Ostrow Street, San Diego, CA 92111; †Department of Surgery, University of California, 200 West Arbor Drive, San Diego, CA 92103-8220; and ‡Department of Biology, Massachusetts Institute of Technology, 77 Massachusetts Avenue, Cambridge, MA 02139-4307

Contributed by Sheldon Penman, January 16, 2002

Mouse tumor models have undergone profound improvements in the fidelity of emulating human disease. Replacing ectopic s.c. implantation with organ-specific orthotopic implantation reproduces human tumor growth and metastasis. Strong fluorescent labeling with green fluorescent protein along with inexpensive video detectors, positioned externally to the mouse, allows the monitoring of details of tumor growth, angiogenesis, and metastatic spread. However, the sensitivity of external imaging is limited by light scattering in intervening tissue, most especially in skin. Opening a reversible skin-flap in the light path markedly reduces signal attenuation, increasing detection sensitivity many-fold. The observable depth of tissue is thereby greatly increased and many tumors that were previously hidden are now clearly observable. This report presents tumor images and related quantitative growth data previously impossible to obtain. Single tumor cells, expressing green fluorescent protein, were seeded on the brain image through a scalp skin-flap. Lung tumor microfoci representing a few cells are viewed through a skin-flap over the chest wall, while contralateral micrometastases were imaged through the corresponding skin-flap. Pancreatic tumors and their angiogenic microvessels were imaged by means of a peritoneal wall skin-flap. A skin-flap over the liver allowed imaging of physiologically relevant micrometastases originating in an orthotopically implanted tumor. Single tumor cells on the liver arising from intraportal injection also were detectable. Possible future technical developments are suggested by the image, through a lower-abdominal skin-flap, of an invasive prostate tumor expressing both red and green fluorescent proteins in separate colonies.

skin-flap window | GFP | RFP | micrometastasis | dormancy

Animal models of human cancer have undergone profound improvements. For many years these simply consisted of ectopic, s.c. implantation of human tumors into immunodeficient mice. Such models usually differed radically from the original donor tumor. For example, such tumors were usually encapsulated (unlike most donor tissue), had radically altered growth characteristics, and, most importantly, did not exhibit metastatic behavior. Also, the important early stages of tumor development were essentially hidden.

Among the attempts to overcome these limitations were skinfold chambers, intravital microscopy of exteriorized organs, and s.c. windows composed of semitransparent material (1–3). However, none of these techniques have been widely adopted because they are suitable primarily for ectopic models and for relatively short periods of observation. One application of the dorsal skin chamber in mice used two-photon confocal microscopy to examine tumor gene expression, angiogenesis, and physiology in a green fluorescent protein (GFP)-expressing tumor (1). Such studies are, however, limited to the ectopic primary tumor and can provide only limited information. Another approach was intravital microscopy of GFP-expressing tumors on exteriorized organs (3). However, the serious morbidity of the procedure precluded long-term spatial-temporal studies.

The greatest fidelity to donor cancer tissue was achieved with GFP models employing orthotopically implanted tumors (4–14). These tumors closely emulate the metastatic behavior of the donor in rate and seed similar target tissues. Also, the GFP-expressing tumors were sufficiently bright that they often could be viewed through simple video equipment situated externally to the animal (13). However, the sensitivity of tumor visualization was limited by absorption through overlying tissue and worked best for relatively shallow tumors. In this report, we shall show that much of this absorption is caused by scattering in the skin. The simple expedient of introducing a minimally invasive, reversible skin flap can increase sensitivity of detection, often by an order of magnitude or more. This increase makes possible direct observation of tumor growth and metastasis as well as tumor angiogenesis and gene expression. The images revealed the microscopic stages of tumor growth and metastatic seeding, often down to the single-cell level, as well as later stages of tumor spread and angiogenesis. Perhaps most importantly, the ability to follow tumor cells in a relatively noninvasive manner in the intact animal makes possible previously unobtainable precision in the studies of tumor behavior and response to chemotherapeutic agents.

Materials and Methods

Expression Vectors. The pLEIN and $pLNCX_2$ vectors were purchased from CLONTECH. The pLEIN vector expresses enhanced green fluorescent protein and the neomycin resistance gene on the same bicistronic message that contains an internal ribosome expression site. The $pLNCX_2$ vector contains the neomycin resistance gene for antibiotic selection in eukaryotic cells (13–15). The red fluorescent protein (RFP; DsRed2, CLONTECH; ref. 16) was inserted in the $pLNCX_2$ vector at the Egl II and *Not*I sites.

GFP Vector Production. For retroviral transduction, PT67, an NIH 3T3-derived packaging cell line expressing the 10 Al viral envelope, was purchased from CLONTECH. PT67 cells were cultured in DMEM (Irvine Scientific) supplemented with 10% (vol/vol) heat-inactivated FBS (Gemini Biological Products, Calabasas, CA). For vector production, packaging cells (PT67) at 70% confluence were incubated with a precipitated mixture of DOTAP transfection reagent (*N*-[1-(2,3-dioleoyloxy)propyl]-*N,N,N*-trimethylammonium methylsulfate; Roche Molecular Biochemicals) and saturating amounts of pLEIN for 18 h. Fresh medium was replenished at this time. The cells were examined by fluorescence microscopy 48 h after transfection. For selection, the cells were cultured in the

Abbreviations: GFP, green fluorescent protein; RFP, red fluorescent protein; SOI, surgical orthotopic implantation.

§To whom reprint requests should be addressed. E-mail: all@anticancer.com.

The publication costs of this article were defrayed in part by page charge payment. This article must therefore be hereby marked "*advertisement*" in accordance with 18 U.S.C. §1734 solely to indicate this fact.

 www.pnas.org/cgi/doi/10.1073/pnas.052029099

presence of 500–2,000 μg/ml of G418 increased in a step-wise manner (Life Technologies, Grand Island, NY) for 7 days.

GFP Gene Transduction of Human and Animal Tumor Cell Lines. For GFP gene transduction, 20–40% confluent human and animal tumor cells were incubated with a 1:1 precipitated mixture of retroviral supernatants of PT67 cells and RPMI medium 1640 or other culture media (GIBCO) containing 10% (vol/vol) FBS (Gemini Biological Products) for 72 h. Human U87 glioma tumor cells, mouse Lewis lung carcinoma cells, human BxPC-3 pancreatic carcinoma cells, and rat Dunning prostate carcinoma cells were incubated with a 1:1 precipitated mixture of retroviral supernatants of PT67 cells and RPMI medium 1640 containing 10% (vol/vol) FBS (Gemini Biological Products) for 72 h. Fresh medium was replenished at this time. Tumor cells were harvested with trypsin/EDTA and subcultured at a ratio of 1:15 into selective medium that contained 50 μg/ml of G418. The level of G418 was increased to 800 μg/ml in a step-wise manner. Clones expressing GFP were isolated with cloning cylinders (Bel-Art Products) by trypsin/EDTA and were amplified and transferred by conventional culture methods in the absence of selective agent.

RFP Gene Transformation. Dunning prostate cancer cells were cultured in RPMI medium 1640 (GIBCO) containing 10% (vol/vol) FBS (Gemini Biological Products). For expression-vector transfection, near-confluent Dunning cells were incubated with a precipitated mixture of Lipofectamine Plus (GIBCO) and saturating amounts of the RFP-expressing pLNCX$_2$-DsRed2 plasmid for 6 h before being replenished with fresh medium. Dunning cells were harvested with trypsin/EDTA 48 h after transfection and subcultured at a ratio of 1:15 into selective medium that contains 200 μg/ml of G418. Cells with stably integrated plasmids were selected by growing transiently transfected cells in 200 μg/ml of G418-containing medium. Clones were isolated with cloning cylinders (Bel-Art Products) by trypsin/EDTA and were amplified and transferred using conventional culture methods in the absence of selective agent.

s.c. Tumor Stock. To have growing tumor tissue stock for subsequent orthotopic implantation, six-week-old *nu/nu* female mice were injected s.c. with a single dose of 10^6–10^7 GFP- or RFP-expressing human or animal tumor cells. Cells were first harvested by trypsinization, washed three times with cold serum-containing medium, and then kept on ice. Cells were injected in the s.c. space of the flank of the animal in a total volume of 0.2–0.4 ml within 40 min of harvesting. The nude mice were killed to harvest tumor tissue 3 to 6 weeks after tumor cell injection for surgical orthotopic implantation (SOI) of tumor fragments (see below).

Brain Cancer Model. The parietal bone of the skull was exposed after an arc-shaped scalp incision. Twenty microliters containing 5×10^5 U87-GFP cells per mouse was injected into the right parietal lobe of the brain with a 1-ml 27G1/2 latex-free syringe (Becton Dickinson). The incision in the scalp was closed with a 7–0 surgical suture in one layer. The animals were kept under isoflurane anesthesia (Iso-Thesia, Vetus Animal Health, Burns Veterinary Supply, Rockville Center, NY) during surgery.

Lung Cancer Model. Tumor pieces (1 mm^3) from s.c.-growing GFP-expressing Lewis lung carcinoma were implanted by SOI onto the left visceral pleura of nude mice (17). The mice were anesthetized by isoflurane inhalation. A small 1-cm transverse incision was made on the left-lateral chest of the nude mice through the fourth intercostal space. A small incision provided access to the pleural space and resulted in total lung collapse. Two tumor pieces were sewn together with an 8–0 nylon surgical suture (Look, Norwell, MA) and fixed by making one knot. The lung was taken up by forceps, and the tumor pieces were sewn into the lower part of the lung with one suture. The lung tissue then was returned into the chest cavity, and the chest muscles and skin were closed with a single layer of 6–0 silk sutures. The lung was reinflated by withdrawing air

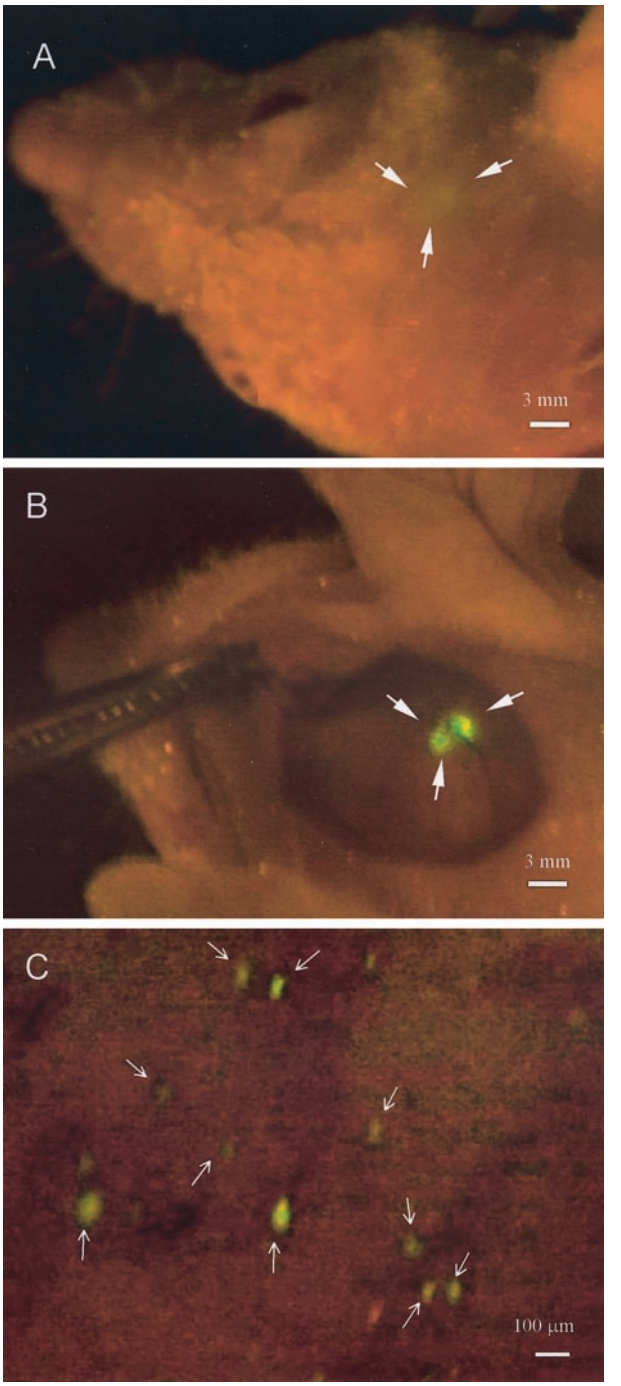

Fig. 1. Whole-body and direct view of macro and microfocal tumors in the brain. (*A*) Whole-body external imaging through the scalp of the bolus of U87-GFP tumor cells immediately after inoculation of tumor cells. The imaged area was ≈2 mm in diameter. (Bar = 3 mm.) (*B*) The scalp-flap window enabled direct view of the bolus of U87-GFP tumor cells immediately after inoculation of tumor cells. The imaged area was ≈2 mm in diameter. (Bar = 3 mm.) (*C*) Direct view of single tumor cells that separated from the bolus via the scalp-flap window. (Bar = 100 μm.) See *Materials and Methods* for details.

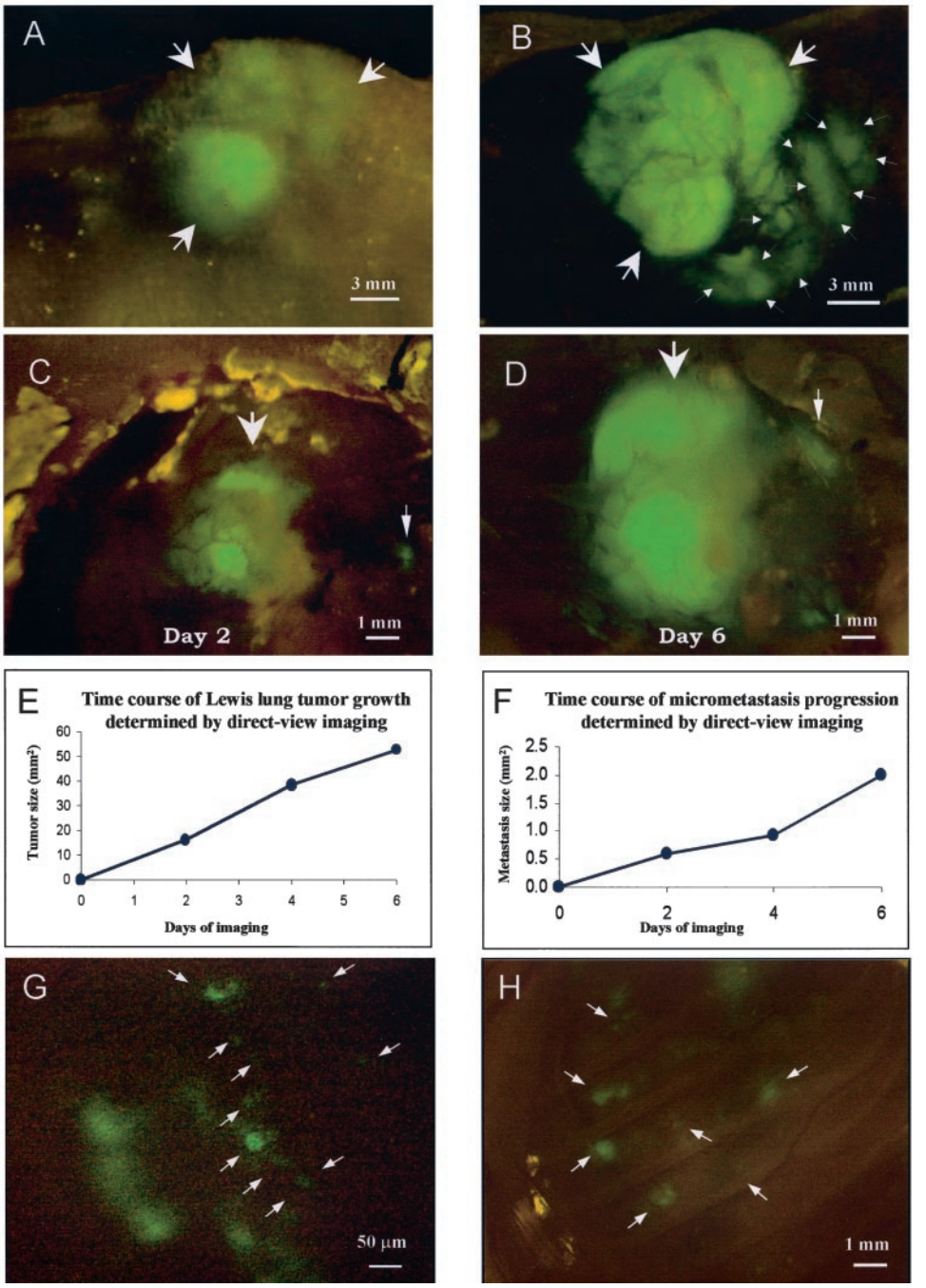

Fig. 2. Whole-body and direct view of lung cancer. (*A*) Whole-body transcutaneous image of orthotopically growing Lewis lung tumor (arrows) in an intact live mouse on day 14 after SOI. (Bar = 3 mm.) (*B*) Direct view of orthotopically growing Lewis lung tumor via skin-flap window also imaged in *A* (arrows). The primary tumor (large arrows) and invading tumor cells (small arrows) are visible. Vessels also can be visualized in the primary tumor. (Bar = 3 mm.) (C) Direct view of microfoci (arrows) on the ipsilateral lung on day 5 after SOI. (Bar = 1 mm.) (*D*) Same as *C*, day 9 after SOI. (Bar = 1 mm.) (*E*) Growth curve of large tumor determined by direct-view images (*C* and *D*, indicated by thick arrows). (*F*) Growth curve of microfocal tumor determined by direct-view images (*C* and *D*, indicated by fine arrows). (*G*) Two three-cell microfoci in the ipsilateral lung at day 5 after SOI visualized by direct-view imaging. (Bar = 50 μm.) (*H*) Micrometastases (arrows) in the contralateral lung at day 7 after SOI visualized by direct-view imaging. (Bar = 1 mm.) See *Materials and Methods* for details.

from the chest cavity with a 23-gauge needle. All procedures of the operation described above were performed with a 7× dissection microscope (MZ6, Leica, Deerfield, IL).

Liver-Metastases Models. *Spontaneous liver-metastasis model.* Tumor fragments (1 mm^3) from the liver-metastatic AC3488 tumor stably expressing GFP were implanted by SOI on the colon in nude mice. After proper exposure of the colon after a lower midline abdominal incision, the serosa of the colon was removed and two pieces of 1 mm^3 tumor fragments per mouse were implanted. An 8–0 surgical suture was used to penetrate these small tumor pieces and suture them on the wall of the colon, which then was returned to the abdominal cavity. The incision in the abdominal wall was closed with a 7–0 surgical suture in one layer (12). The animals were anesthetized during surgery with a ketamine-mixture of Ketaset and PromAce (both from Fort Dodge Laboratories, Fort Dodge,

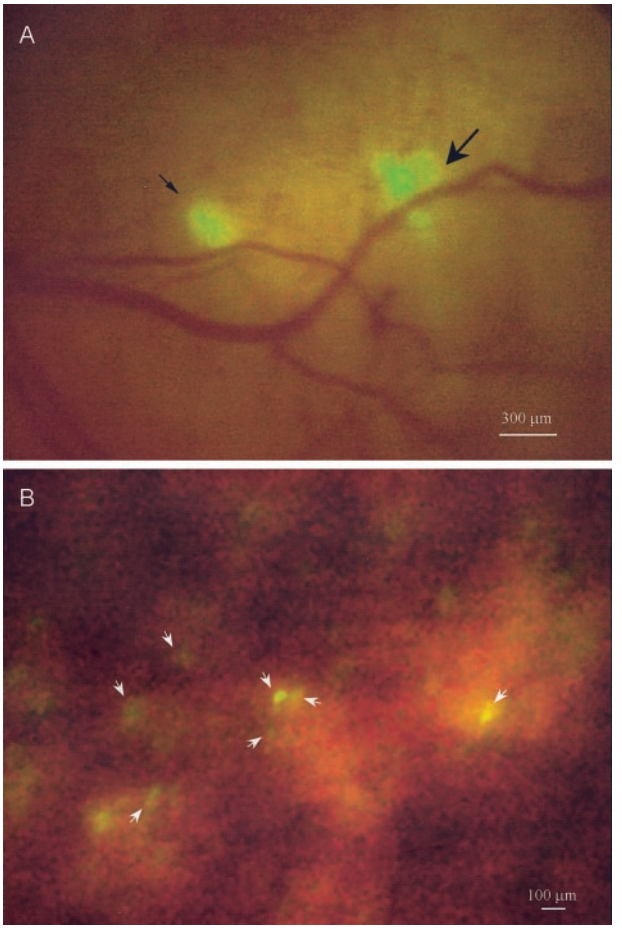

Fig. 3. Direct view of colon cancer liver micrometastasis. (*A*) Ventral direct view of micrometastasis of AC3488-GFP in the right lobe of the liver via a skin-flap window over the upper abdominal wall at day 7 after SOI. The smaller micrometastasis is ≈150 μm in diameter (fine arrow), and the larger is ≈300 μm in diameter (thick arrow). (*B*) Direct view of single cells (arrows) in right lobe of the liver after intraportal injection of 10^6 Colo-320 GFP cells. (Bar = 100 μm.) See *Materials and Methods* for details.

IA) and Xylazine HCl (American Animal Health, Wisner, NE). All procedures were performed with the 7× dissection microscope.

Experimental liver-metastasis model. Colo 320-GFP cells first were harvested by trypsinization and washed three times with cold serum-free medium. After proper exposure of the portal vein after an upper midline abdominal incision, 100 μl containing 10^6 GFP cells were injected in the portal vein with a 1-ml 39G1 latex-free syringe (Becton Dickinson). The puncture hole in the portal vein was pressed for about 10 s with a sterile cotton bar to prevent bleeding. The incision in the abdominal wall was closed with a 7–0 surgical suture in one layer. The animals were kept under the ketamine-mixture anesthesia during surgery. All procedures of the operation described above were performed with the 7× dissection microscope.

Pancreatic Cancer Model. The Bx-PC-3 human pancreatic tumor, expressing GFP and grown s.c. in nude mice, was resected aseptically. Necrotic tissues were cut away, and the remaining healthy tumor tissues were cut with scissors and minced into ≈1-mm^3 pieces in Hanks' balanced salt solution containing 100 units per ml of penicillin and 100 units per ml of streptomycin. Mice were anesthetized by the ketamine-mixture. The abdomen was sterilized with alcohol. An incision then was made through the left upper abdominal pararectal line and peritoneum. The pancreas was carefully exposed, and three tumor pieces were transplanted on the middle of the pancreas with a 6–0 Dexon (Davis-Geck, Manati, Puerto Rico) surgical suture. The pancreas then was returned into the peritoneal cavity, and the abdominal wall and the skin were closed with 6–0 Dexon sutures. Animals were kept in a sterile environment. All procedures of the operation described above were performed with the 7× dissection microscope (18).

Prostate Cancer Model. Tumor tissue used for surgical orthotopic implantation was derived from a tumor growing s.c. after injection of Dunning prostate carcinoma-GFP or Dunning prostate carcinoma-RFP tumor cells in nude mice. Tissue from the periphery of the tumor was harvested in log phase, and necrotic tissue was carefully removed. The viable tissue then was cut into small cubes of 1 mm^3 in standard tissue culture medium under sterile conditions. To minimize variation in subsequent tumor growth and metastasis, these tumor pieces were randomly mixed, and an equal amount was implanted in each mouse as described below. Mice were anaesthetized with the ketamine-mixture and positioned supinely. An arc-shaped skin flap was made right above the pubis symphysis to expose the prostate gland. The fascia surrounding the ventral portion of the prostate was carefully isolated, and the two ventral lateral lobes of the gland were exposed by a small incision using a pair of fine surgical scissors. One piece of Dunning GFP tissue was sutured into one lobe with an 8–0 nylon suture. Similarly, one piece of Dunning RFP tissue was sutured into the other lobe. The abdomen was closed with a 6–0 suture (19). All procedures of the operation were performed with the 7× dissection microscope.

Skin-Flap Windows. Tumor cells on the various internal organs were visualized through the skull or body wall through different skin-flap windows over the scalp, chest wall, upper abdomen, and lower abdomen. The animals were anesthetized with the ketamine-mixture. An arc-shaped incision was made in the skin, and s.c. connective tissue was separated to free the skin flap. The skin flap could be opened repeatedly to image tumor cells on the internal organs through the nearly transparent mouse body walls or skull and simply closed with an 6–0 suture. This procedure greatly reduced the scatter of fluorescent photons.

Fluorescence Imaging. A Leica fluorescence stereo microscope model LZ12 equipped with a mercury 50W lamp power supply was used (13–15, 20). To visualize both GFP and RFP fluorescence at the same time, excitation was produced through a D425/60 band pass filter, 470 DCXR dichroic mirror, and emitted fluorescence was collected through a long pass filter GG475 (Chroma Technology, Brattleboro, VT). Macroimaging was carried out in a light box (Lightools Research, Encinitas, CA). Fluorescence excitation of both GFP and RFP tumors was produced through an interference filter 440+/−20 nm using slit fiber optics for animal illumination. Fluorescence was observed through a 520-nm long pass filter. Images from the microscope and light box were captured on a Hamamatsu C5810 3-chip Cool-Color charge-coupled device camera (Hamamatsu Photonics, Hamamatsu City, Japan).

Images were processed for contrast and brightness and analyzed with the use of IMAGE PRO PLUS v.4.0 software (Media Cybernetics, Silver Spring, MD). High resolution images of 1024 × 724 pixels were captured directly on an IBM PC or continuously through video output on a high-resolution Sony VCR model SLV-R1000 (Sony, Tokyo; refs. 13–15).

All animal studies were conducted in accordance with the principles and procedures outlined in the National Institute of Health Guide for the Care and Use of Animals under assurance number A3873–1. Animals were kept in a barrier facility (12). Mice

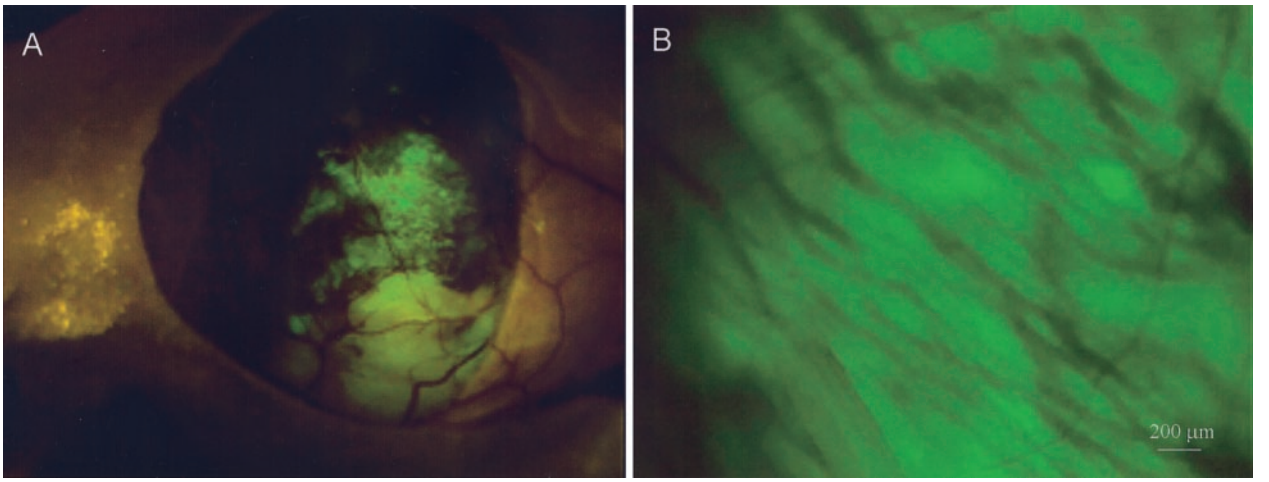

Fig. 4. Direct view of microvessels of orthotopically growing pancreatic cancer. (*A*) The human Bx PC-3-GFP pancreatic tumor, microvessels, and metastasis to the spleen (fine arrows) were directly viewed via a skin-flap window over the abdominal wall of a nude mouse at day 58 after SOI. (*B*) Microvessels were directly viewed and highly resolved through the skin-flap window at higher magnification. (Bar = 200 μm.) See *Materials and Methods* for details.

were fed with autoclaved laboratory rodent diet Tecklad LM-485 (Western Research Products, Orange, CA).

Results

Optical Efficacy of the Skin Flap. Fig. 1 shows the direct view images of a fluorescent brain tumor. U87-GFP cells were inoculated on to the right parietal lobe of the brain. Fig. 1*A* shows the image obtained through the skull and scalp. Fig. 1*B* shows the same preparation but with the scalp open via a skin flap. Quantitative measurement of the fluorescence shows a twenty-fold increase in intensity when the intervening scalp tissue is removed. Fig. 1*C* shows an adjoining area in which single fluorescent cells are clearly resolved and which could not be imaged through the scalp.

Quantitative Imaging of Lung Cancer Microfoci. A powerful advantage conferred by the skin-flap technique is the opportunity to return to the same tumor and obtain quantitative measurements over time. The relatively modest invasiveness and low morbidity of the technique allows meaningful long-term measurements. An example of such an application is afforded by the data in Fig. 2. Lewis lung-GFP was implanted on the ipsilateral lung by SOI. The whole-body image through the skin (Fig. 2*A*) was compared with the external direct-view images obtained through a skin-flap window over the chest wall (Fig. 2*B*). The direct-view image allows fine details such as tumor microfoci and angiogenic vessels on the primary tumor to be imaged, which is not possible through the skin. Images of primary tumor and microfoci progression were recorded over a 6-day period (Fig. 2 *C* and *D*), and tumor growth curves were constructed (Fig. 2 *E* and *F*). The congruence between the data points and the expected growth curve suggests that the technique yields accurate quantitative measurements. Microfoci as small as one or two cells on the ipsilateral lung could be clearly imaged through the skin flap on day 5 (Fig. 2*G*). Similarly, microfoci seeded by metastasis from the ipsilateral lung were directly imaged by means of a skin-flap window over the contralateral lung on day 7 (Fig. 2*H*).

External Direct View Images of Liver Micrometastasis. AC3488-GFP, when implanted orthotopically in mice, mimics a common behavior of colon cancer, i.e., metastasis to liver. Metastatic microfoci were clearly visible by day 7 after implantation. Two metastatic lesions of 150 μm and 300 μm in diameter were externally imaged through a skin-flap window over the abdominal wall of the mouse (Fig. 3*A*). The 150 μm metastatic lesion appeared to be formed by a single tumor microfocus, whereas the 300 μm lesion appeared to be separable into five separate colonies. The largest of these colonies, approximately 130 μm in diameter, was located in the center of the metastatic lesion. Closely associated were the other four smaller microfoci that ranged in size from 80 to 100 μm in diameter. These satellite microfoci may have arisen through separate metastatic events.

Another model of metastatic spread is the intraportal injection of cells of GFP-expressing colon cancer line, colo-320. Microfoci and even single cells were clearly visible in the liver when externally viewed through a skin-flap window (Fig. 3*B*).

Imaging Orthotopically Growing Pancreatic Cancer and Its Angiogenic Microvessels. One of the less obvious properties of the fluorescent orthotopic model is the ability to image induced angiogenic microvessels. This ability is made possible, in part, by the extensive angiogenic microvessel induction when tumors are implanted orthotopically. Also, the brilliance of the tumor fluorescence, facilitated by the reduced absorption through the skin-flap window, allows imaging of the induced microvessels as

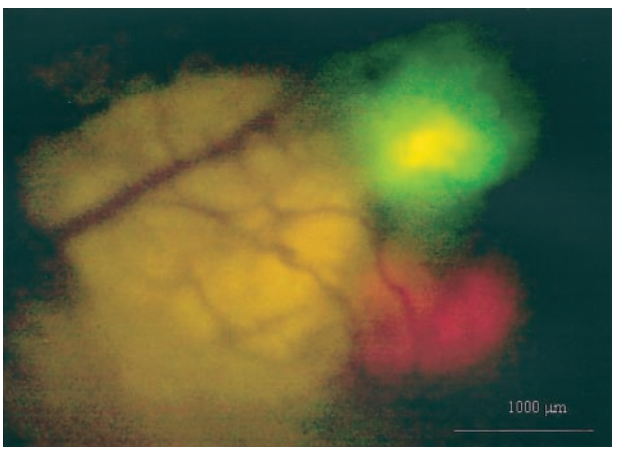

Fig. 5. Dual-color direct view of Dunning-GFP and Dunning-RFP. Dual-color green and red fluorescent direct-view image of the Dunning-GFP tumor growing on the left lateral lobe and Dunning-RFP tumor growing on right lateral lobe of the mouse prostate via a lower abdominal wall skin-flap window one day after SOI. (Bar = 1 mm.) See *Materials and Methods* for details.

dark against a bright background. Fig. 4 shows the orthotopically growing BxPC 3-GFP human pancreatic tumor surrounded by its microvessels visible by their dark shadows.

Dual Color External Direct-View Imaging. The development of other fluorescence colors opens up many new possibilities of experimental design. The ability to image simultaneous green and red fluorescence was shown in Fig. 5. Dunning prostate RFP and GFP tumors were implanted on separate lobes of the nude mouse prostate. A ventral skin flap allowed external direct-view imaging of the GFP tumor growing on the left lateral lobe and the RFP labeled tumor on the right lateral lobe. Both tumors were less than 1 mm in diameter. Some of the potential of dual labeling is suggested in *Discussion* below.

Discussion

This report demonstrates a previously unobtainable sensitivity for external imaging of internal fluorescent tumors. The improvement in sensitivity afforded by the skin-flap window now permits imaging on essentially any internal organ of animals at least mouse-sized. In many cases, single cells can be visualized, thus allowing study of the earliest events in tumor establishment. Similarly, micrometastases of one to two cells were visualized on the lung and on the liver, allowing study of the earliest events in metastatic colonization. The quantitative time-course studies reported here illustrate the feasibility of obtaining precise growth data. These will permit accurate, rapid and economical assessment of new chemotherapeutic agents.

Angiogenesis has become one of the most intense areas of cancer research; studies attest to its crucial role in tumor growth and metastasis. Such data are central to understanding phenomena such as interference of the primary tumor of metastatic growth (21, 22) and, most importantly, the effect of chemotherapeutic agents on angiogenic vessels. However, obtaining precise data relating angiogenesis to tumor growth and metastasis is difficult as long as animal killing is required for each measurement. The fluorescent orthotopic metastatic model affords a relatively noninvasive method of visualizing angiogenic vessel induction, in both space and time, for primary and metastatic tumors. Fig. 4 shows angiogenic vessels anastomosing the mouse pancreas. These vessels appear as dark shadows against the background of a brilliant fluorescent tumor. The microvessels were directly visualized through a skin-flap window on the peritoneal wall. The vessel development can be closely followed and quantified in real time, allowing precise answers to the relation of angiogenesis and cancer progression. The technique also affords rapid evaluation of drugs that may affect development of these vessels. Of special interest is the very low morbidity associated with the technique, which allows tumors to be followed for long periods of time.

An especially intriguing and currently little understood phenomenon is that of interference between disparate tumors. Apparently, the presence of a primary tumor can suppress the growth, angiogenesis, or metastasis of a second distinct tumor (21, 22). Research into tumor interference has largely used ectopic tumors such as s.c. xenografts or intraportally injected second tumor populations. The externally viewed, fluorescent orthotopic tumor model affords several new and powerful approaches to this question. Tumors can be placed into their natural environments and allowed to grow without surgical interference. Secondly, and most important, tumors can be labeled in two colors, which allows great flexibility in placement and timing of the tumors, which can then be followed for growth and angiogenesis for an unlimited period.

The external direct imaging by means of a skin-flap window of GFP- and RFP-labeled tumor cells affords extraordinarily high resolution, down to single cells, with a small investment in a light source and detection equipment. In contrast, luciferase based bioluminescence assays are two to three orders of magnitude less sensitive, they cannot detect single tumor cells, and they require both elaborate equipment and restraint of the experimental animal (23). The system described here is capable of multicolor fluorescence and affords a unique approach to the study of the critical factors in cancer progression.

This study was supported in part by National Cancer Institute Grant 1R43CA89779-01.

1. Brown, E. B., Campbell, R. B., Tsuzuki, Y., Xu, L., Carmeliet, P., Fukumura, D. & Jain, R. K. (2001) *Nat. Med.* **7**, 864–868.
2. Ciancio, S. J., Coburn, M. & Hornsby, P. J. (2000) *J. Surg. Res.* **92,** 228–232.
3. Naumov, G. N., Wilson, S. M., MacDonald, I. C., Schmidt, E. E., Morris, V. L., Groom, A. C., Hoffman, R. M. & Chambers, A. F. (1999) *J. Cell Sci.* **112,** 1835–1842.
4. Chishima, T., Miyagi, Y., Wang, X., Yamaoka, H., Shimada, H., Moossa, A. R. & Hoffman, R. M. (1997) *Cancer Res.* **57,** 2042–2047.
5. Chishima, T., Miyagi, Y., Wang, X., Tan, Y., Shimada, H., Moossa, A. R. & Hoffman, R. M. (1997) *Anticancer Res.* **17,** 2377–2384.
6. Chishima, T., Miyagi, Y., Wang, X., Baranov, E., Tan, Y., Shimada, H., Moossa, A. R. & Hoffman, R. M. (1997) *Clin. Exp. Metastasis* **15,** 547–552.
7. Chishima, T., Miyagi, Y., Li, L., Tan, Y., Baranov, E., Yang, M., Shimada, H., Moossa, A. R. & Hoffman, R. M. (1997) *In Vitro Cell. Dev. Biol* **33,** 745–747.
8. Chishima, T., Yang, M., Miyagi, Y., Li, L., Tan, Y., Baranov, E., Shimada, H., Moossa, A. R., Penman, S. & Hoffman, R. M. (1997) *Proc. Natl. Acad. Sci. USA* **94,** 11573–11576.
9. Yang, M., Hasegawa, S., Jiang, P., Wang, X., Tan, Y., Chishima, T., Shimada, H., Moossa, A. R. & Hoffman, R. M. (1998) *Cancer Res.* **58,** 4217–4221.
10. Yang, M., Jiang, P., Sun, F. X., Hasegawa, S., Baranov, E., Chishima, T., Shimada, H., Moossa, A. R. & Hoffman, R. M. (1999) *Cancer Res.* **59,** 781–786.
11. Yang, M., Jiang, P., An, Z., Baranov, E., Li, L., Hasegawa, S., Al-Tuwaijri, M., Chishima, T., Shimada, H., Moossa, A. R. & Hoffman, R. M. (1999) *Clin. Cancer Res.* **5,** 3549–3559.
12. Hoffman, R. M. (1999) *Invest. New Drugs* **17,** 343–359.
13. Yang, M., Baranov, E., Jiang, P., Sun, F.-X., Li, X.-M., Li, L., Hasegawa, S., Bouvet, M., Al-Tuwaijri, M., Chishima, T., *et al.* (2000) *Proc. Natl. Acad. Sci. USA* **97,** 1206–1211.
14. Yang, M., Baranov, E., Li, X.-M., Wang, J.-W., Jiang, P., Li, L., Moossa, A. R., Penman, S. & Hoffman, R. M. (2001) *Proc. Natl. Acad. Sci. USA* **98,** 2616–2621.
15. Yang, M., Baranov, E., Moossa, A. R., Penman, S. & Hoffman, R. M. (2000) *Proc. Natl. Acad. Sci. USA* **97,** 12278–12282.
16. Bevis, B. J. & Glick, B. S. (2002) *Nat. Biotechnol.* **20,** 83–87.
17. Rashidi, B., Yang, M., Jiang, P., Baranov, E., An, Z., Wang, X., Moossa, A. R. & Hoffman, R. M. (2000) *Clin. Exp. Metastasis* **18,** 57–60.
18. Bouvet, M., Yang, M., Nardin, S., Wang, X., Jiang, P., Baranov, E., Moossa, A. R. & Hoffman, R. M. (2000) *Clin. Exp. Metastasis* **18,** 213–218.
19. An, Z., Wang, X., Geller, J., Moossa, A. R. & Hoffman, R. M. (1998) *Prostate* **34,** 169–174.
20. Zhao, M., Yang, M., Baranov, E., Wang, X., Penman, S., Moossa, A. R. & Hoffman, R. M. (2001) *Proc. Natl. Acad. Sci. USA* **98,** 9814–9818.
21. Kisker, O., Onizuka, S., Banyard, J., Komiyama, T., Becker, C. M., Achilles, E. G., Barnes, C. M., O'Reilly, M. S., Folkman, J. & Pirie-Shepherd, S. R. (2001) *Cancer Res.* **61,** 7298–7304.
22. Guba, M., Cernaianu, G., Koehl, G., Geissler, E. K., Jauch, K. W., Anthuber, M., Falk, W. & Steinbauer, M. (2001) *Cancer Res.* **61,** 5575–5579.
23. Sweeney, T. J., Mailander, V., Tucker, A. A., Olomu, A. B., Zhang, W., Cao, Y., Negrin, R. S. & Contag, C. H. (1999) *Proc. Natl. Acad. Sci USA* **96,** 12044–12049.